Research Paper

# Effect of Trichostatin A on Bleomycin Induced Pulmonary Fibrosis in Mice and its Mechanism

QIAN ZHANG*, ZE XIN GUO[1], JING ZHANG[1], D. L. YANG[2], P. JIANG, J. CAO[1] AND S. LI[1]

Department of Respiratory and Critical Care Medicine, The First Central Hospital Affiliated to Nankai University, [1]Department of Respiratory and Critical Care Medicine, Tianjin Medical University General Hospital, Heping, Tianjin 300052, [2]Department of General Education Courses, Cangzhou Medical College, Yunhe, Hebei 061000, China



**To investigate the effect and mechanism of trichostatin A on bleomycin induced pulmonary fibrosis in mice compared with dexamethasone and pirfenidone is the objective of the study. C57 black 6 mice were instilled intranasal bleomycin to establish pulmonary fibrosis model. They were divided into five groups: Control group, model group, dexamethasone group, pirfenidone group and trichostatin A group. Hematoxylin and eosin staining and Masson's staining was conducted; the expression of related proteins in each group was observed by immunohistochemistry and Western blotting. Hematoxylin and eosin staining and Masson's staining showed that the lung tissue was damaged in varying degrees, interstitial protein deposition, basal cell hyperplasia and a large number of macrophage infiltration in the alveolar cavity. The lung tissue injury in trichostatin A group was the least. The expression of vimentin, collagen-I, alpha smooth muscle actin and other interstitial proteins in the model group increased significantly, and the expression of above interstitial proteins in each intervention treatment group decreased in varying degrees, especially in trichostatin A group. The expression of suppressor of mothers against decapentaplegic homolog 7 protein decreased significantly in the model group and increased significantly in the trichostatin A group; there was no significant difference in the expression of p38-mitogen-activated protein kinase protein in each group. The expression of interstitial protein messenger RNA such as vimentin, collagen-I and alpha smooth muscle actin peaked on the 14$^{th}$ d after modeling. Trichostatin A could significantly inhibit the progression of pulmonary fibrosis by inhibiting the activity of histone deacetylase 1, while histone deacetylase 1 could activate transforming growth factor beta-1/suppressor of mothers against decapentaplegic pathway, involved in the progression of pulmonary fibrosis. Dexamethasone could not delay or improve pulmonary fibrosis, or even aggravate the progression of pulmonary fibrosis.**

**Key words: Pulmonary fibrosis, trichostatin A, histone deacetylase 1, transforming growth factor-beta 1/ suppressor of mothers against decapentaplegic pathway**

Pulmonary fibrosis is caused by various reasons, such as epithelial cell injury on the alveolar surface, a large number of inflammatory cell infiltration, fibroblast proliferation and a large amount of extracellular matrix protein deposition. These pathogenic factors can be due to the stimulation of poisons, spontaneous immune response, adverse drug reaction, infection and other factors, which eventually lead to the structural changes and functional loss of normal lung tissue. In recent years, the incidence rate of pulmonary fibrosis has increased significantly. Treatment is extremely difficult. Traditional glucocorticoids have little curative effect and obvious side effects. Therefore, new methods of treatment need to be explored. Recent studies have shown that the imbalance of Histone Acetyltransferases (HAT)/Histone Deacetylases (HDACs) not only leads to the occurrence of tumors, but also initiates some chronic fibrosis diseases, such as Idiopathic Pulmonary Fibrosis (IPF) and renal interstitial fibrosis[1]. Therefore, the research of HDAC and Histone Deacetylase inhibitor (HDACi) may bring new breakthroughs in the treatment of pulmonary fibers. As a potent, specific and reversible HDACi, Trichostatin A (TSA), takes HDAC as the target and plays different roles by inhibiting the activity of HDAC. It has been reported that

***Address for correspondence**
E-mail: jenna9898@163.com

TSA can promote cell differentiation, block cell growth cycle and induce tumor cell apoptosis by upregulating histone acetylation level in cells, so as to promote the transcription and expression of anti-tumor transcription factors, regulate relevant signal pathways and exert anti-tumor effect[2-12]. So far, TSA has attracted more and more attention in the field of pulmonary fiber disease. This study aims to explore the role and related mechanism of TSA in bleomycin induced C57 Black 6 (C57BL/6) mouse pulmonary fibrosis model[13].

## MATERIALS AND METHODS

### Materials:

60 healthy male C57BL/6 mice, aged 7-8 w and weighing about 20-22 g, were purchased from SBF (Beijing) Biotechnology Co., Ltd. (production license No.: Scxk (Beijing) 2019-0010), bleomycin hydrochloride (Japan Co., Ltd., 600700), pirfenidone (Beijing Kangdini Pharmaceutical Co., Ltd., 20200908) and dexamethasone sodium phosphate injection (Tianjin Jinyao Pharmaceutical Co., Ltd., batch No.: 2005161), hydroxyproline detection kit (Solarbio).

### Methods:

**Animal grouping:** 60 healthy C57BL/6 mice were raised in Specific Pathogen Free (SPF) animal room with the temperature of 23°~27°, humidity of 55 %-65 %, 12 h light/dark alternation and adapted to feeding for 7 d. These mice were grouped by random number expression method. The five groups were Model group (MOD), Control group (CON), Dexamethasone group (DEX), Pirfenidone group (PIR) and Trichostatin A group (TSA), 12 in each group, fed in separate cages.

**Establishment and intervention of pulmonary fibrosis model:** The experimental mice were injected intraperitoneally with chloral hydrate (2 ml/kg). After anesthesia, they were fixed on the mouse board in the supine position, keeping their body vertical above the head and below the tail. They held a micropipette in their right hand and dropped bleomycin (5 mg/kg) into their nostrils 200 µl of solution per mouse. If the mice breathe normally and gradually inhale the liquid, they can continue the nasal drip operation. After the administration, they are fed continuously. On the next day, they are given DEX (3 mg/kg/d, intraperitoneal injection), PIR (300 mg/kg/d, intragastric injection) and TSA (40 mg/kg/d, intraperitoneal injection). The mice in each group were fed with standard feed and free drinking water. Four mice in each group were randomly killed on the 7th, 14th and 28th d after modeling.

### Specimen collection and treatment:

**Specimen collection:** After the mice were given excessive anesthesia, the lungs were exposed by thoracotomy, blood was taken from the right heart, put into Ethylenediaminetetraacetic Acid (EDTA) anticoagulant tube, Phosphate-Buffered Saline (PBS) was injected from the right ventricle to wash the lungs white and the trachea and lung tissues were separated. The left lung tissue was fixed with paraformaldehyde (4 %) and paraffin sections were prepared. Some were stained with Hematoxylin and Eosin (HE) and Masson's for pathological observation, and the other was stained with immunohistochemistry. The right lung was placed in the Eppendorf (EP) tube and placed in the liquid nitrogen tank for subsequent Western, Polymerase Chain Reaction (PCR) and hydroxyproline detection.

**HE and Masson's staining of lung tissue:** The lung tissue of each group of mice was fixed with paraformaldehyde, dehydrated, embedded in paraffin and routinely sliced to 4 µM. HE and Masson's staining were performed, and the degree of pulmonary fibrosis in each group was observed and evaluated under the microscope.

**Detection of hydroxyproline in lung tissue:** Cut the frozen lung tissue (wet mass 100 mg/piece) into homogenate and detect the tissue Hydroxyproline (HYP) content (pg/g lung tissue) by alkali hydrolysis method. The specific operation shall be carried out in strict accordance with the instructions of HYP detection kit.

**Detection of mouse lung tissue by Western blot:** Alpha Smooth Muscle Actin (α-SMA), vimentin, Transforming Growth Factor-beta 1 (TGF-β1), HDAC1, Suppressor of mothers against decapentaplegic homolog (Smad) 2, phosphorylated Smad2 (p-Smad2), Smad3, p-Smad3, Smad7 and other proteins were expressed. The lung tissue of mice was accurately weighed to 100 mg, cut into pieces, added with tissue protein lysate containing phosphatase inhibitor (containing 2 % protease inhibitor), homogenized, centrifuged at 12 000 rpm for 10 min, collected the supernatant and measured the protein concentration by Bicinchoninic Acid (BCA) method. Take 50 µg of protein which was prepared by Sodium Dodecyl-Sulfate Polyacrylamide Gel Electrophoresis (SDS-PAGE). The membrane was

transferred to 5 % skim milk at room temperature for 90 min and was incubated overnight with first antibody at 4°. Tris-Buffered Saline with Tween-20 (TBST) was washed for 5 times, add the secondary antibody and incubate at room temperature for 60 min and discard the secondary antibody, TBST was washed for 5 times, hypersensitive Enhanced Chemiluminescence (ECL) was developed, gel imaging system was developed, Glyceraldehyde 3-Phosphate Dehydrogenase (GAPDH) was used as reference. The relative expression of the target protein was calculated by software image J.

**Real time fluorescence quantitative PCR was used to detect the expression of vimentin, collagen-I and α-SMA in lung tissue:** Take 50 mg of mouse lung tissue, add 800 µl lysate, grind the tissue thoroughly with a homogenizer, extract the total Ribonucleic Acid (RNA) according to the instructions of RNA Prep pure animal tissue total RNA extraction kit and detect the expression of vimentin, collagen-I, α-SMA and other messenger RNA (mRNA) by real-time fluorescence quantitative PCR. The operation steps are carried out according to the instructions of FastQuant RT kit and SuperReal PreMix Plus kit. Amplification conditions: Pre denaturation at 95° for 5 min; Denaturation at 95° for 10 s, annealing at 60° for 20 s, extension at 72° for 27 s, a total of 40 cycles. There were 4 mice in each group, each with 3 multiple wells. GAPDH was used as the internal reference gene and $2^{-\Delta\Delta CT}$, the relative expression of mRNA was calculated by CT method (Table 1).

**Weighted Gene Co-Expression Network Analysis (WGCNA) model and Kyoto Encyclopedia of Genes and Genomes (KEGG) pathway enrichment analysis:** WGCNA and KEGG pathway enrichment analysis were used to study the differences in clinical characteristics and gene expression patterns among different subgroups of pulmonary fibrosis. High throughput sequencing technology and microarray are increasingly used to study the molecular mechanism of disease subtypes. In order to further explore the genetic and molecular basis of pulmonary fibrosis, we analyzed the differences of molecular mechanism between patients with pulmonary fibrosis and divided pulmonary fibrosis into several subtypes through gene differential expression analysis. WCGNA model and KEGG pathway enrichment analysis were used to study the differences in clinical characteristics and gene expression patterns among different subtypes.

**Statistical analysis:**

The GraphPad Prism 8.0 software was used for statistical analysis. The measurement data were expressed by mean±Standard Deviation (SD) (x±s). One way Analysis of Variance (ANOVA) was used for inter group comparison. Least Significant Difference (LSD) t-test was used for pairwise comparison. The difference was statistically significant with $p<0.05$.

## RESULTS AND DISCUSSION

General situation and death of mice in each group was shown here. After modeling, the activities and diet of mice were basically normal. From the 5$^{th}$ d, mice showed mental depression, slow response, reduced eating and activities. With the passage of time, these manifestations continued to worsen, shortness of breath, significantly reduced body weight compared with that before modeling and there was no death of animals in each group.

Pathological changes of mouse lung tissue were shown here. In CON group, the lungs were pink, smooth and elastic. While, in MOD group, the lung volume was decreased, the surface was not smooth, manifested as nodular, hard, poor elasticity, uneven lung surface, accompanied by bleeding focus and old bleeding.

**TABLE 1: EXPRESSION OF VIMENTIN, COLLAGEN-I AND α-SMA IN LUNG TISSUE BY REAL TIME FLUORESCENCE QUANTITATIVE PCR**

| RT-PCR primer sequence | | |
|---|---|---|
| **Gene name** | **Primer sequence** | |
| α-SMA | Forward | 5'-TGGGCCCTCAAAAGGCTTCG-3' |
| | Reverse | 3'-CGTCGGTAAAGAAAGGCACAC-5' |
| Vimentin | Forward | 5'-CGTCCACACGCACCTACAG-3' |
| | Reverse | 3'-GGGGGATGAGGAATAGAGGCT-5' |
| Collagen-I | Forward | 5'-GCTCCTCTTAGGGGCCACT-3' |
| | Reverse | 3'-ATTGGGGACCCTTAGGCCAT-5' |

At the same time, in DEX group, the lung morphology was normal, but hemorrhagic changes, slight swelling and no obvious nodule appearance were observed. In PIR group, the lung morphology was acceptable, the hemorrhagic changes were reduced and there was no obvious appearance of nodules. In TSA group, the lung morphology was acceptable, without obvious hemorrhagic changes and nodule appearance (fig. 1).

HE staining results were illustrated here. In the CON group, the lung tissue structure was clear, the alveolar septum was clearly visible and there was no exudation and filling in the alveolar cavity. After modeling, the alveolar structure in each group was disordered, bleeding in the alveolar cavity, thickening of alveolar septum, deposition of collagen fibers, proliferation of fibroblasts and proliferation of type II alveolar epithelial cells were observed in the lung stroma; with the extension of time, a large number of basal cell hyperplasia and macrophage infiltration appeared, especially in the MOD group and DEX group, and the least in TSA group (fig. 2).

Masson staining results were illustrated here. In the CON group, the alveolar structure of the lung tissue was complete, the alveolar septum was not widened, there was no collagen fiber deposition and a few blue purple collagen fibers were arranged around the bronchus. After modeling, a large number of blue collagen fibers were deposited in the lung stroma and around the airway in each group, the most in the MOD group and DEX group and the least in TSA group (fig. 3).

Hydroxyproline content test results were illustrated here. After modeling, the content of hydroxyproline in each group was significantly higher than that in the CON group and reached the peak on the 28$^{th}$ d. The content of MOD group and DEX group was significantly higher than that in other groups and the content of TSA group was the least (fig. 4).

Western blot was used to detect the protein expression in the lung tissue of mice in each group. The expressions of collagen-I and vimentin in the MOD group were significantly higher than those in the CON group. In the three drug intervention groups, the expression of proteins above DEX was significantly higher than that in PIR group and TSA group, and the expression of TSA group was the least (fig. 5A). MOD group, α-SMA and TGF-β, the expression of protein in the three drug intervention groups was significantly lower than that in the MOD group (fig. 5B).

The expression of HDAC1 protein in the MOD group was significantly higher than that in the CON group and the expression of HDAC1 protein decreased in different degrees in the three drug intervention groups; there was no significant difference in the expression of Smad2 and Smad3 proteins compared with the CON group (fig. 5C). The expressions of p-Smad2 and p-Smad3 proteins in the MOD group were significantly higher than those in the CON group, and the three drug intervention groups were decreased in varying degrees than those in the MOD group; the expression of Smad7 protein in the MOD group was significantly lower than that in the CON group, and the three drug intervention groups increased in varying degrees than that in the MOD group (fig. 5D).

The expression of Phosphatidylinositol 3-Kinase (PI3K) and Nuclear Factor kappa B (NF-κB) protein in the MOD group was higher than that in the CON group. The expression of the above two proteins in the three drug intervention treatment groups decreased in varying degrees and the expression of NF-κB was the least in TSA group. There was no significant difference in the expression of p38-Mitogen-Activated Protein Kinase (MAPK) among the groups (fig. 5E).

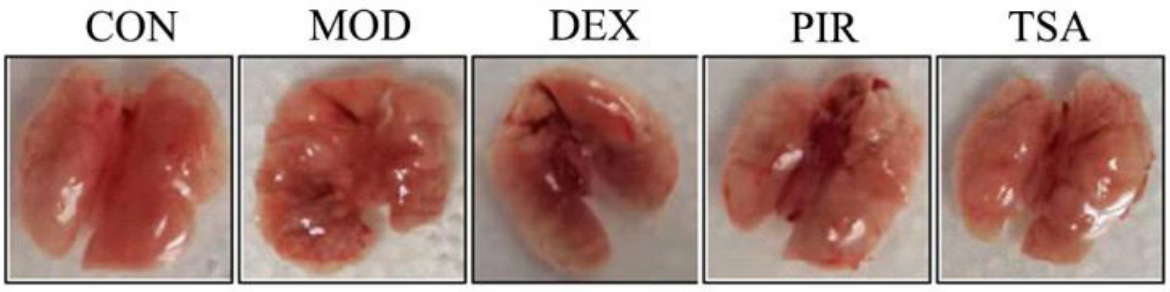


**Fig. 1: Macroscopic observation of lung tissue of mice in each group**

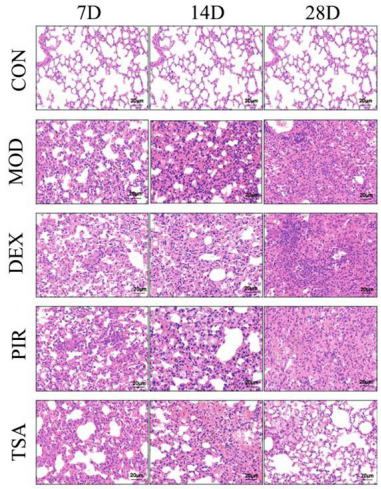


**Fig. 2: Histological lung tissues were stained with HE (200×)**

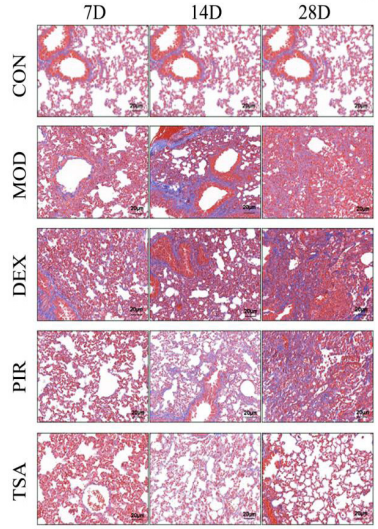


**Fig. 3: Histological sections of mouse lung tissue were stained with Masson (200×)**

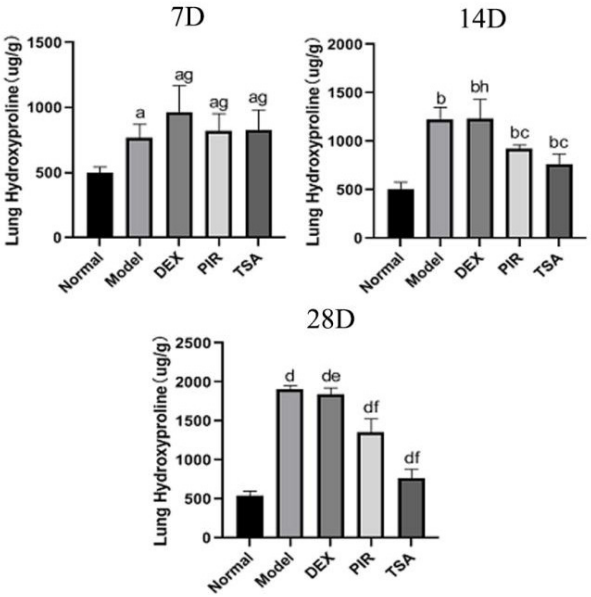


**Fig. 4: The content of hydroxyproline in lung tissue of mice in each group at 7, 14 and 28 d after modeling (pg/g)**
**Note: Values are expressed as mean±SD, [a]p<0.05 *vs.* CON; [g]p<0.05 *vs.* MOD group; [b]p<0.05 *vs.* CON; [c]p<0.05 *vs.* MOD group; [h]p>0.05 *vs.* MOD group; [d]p<0.05 *vs.* MOD group; [e]p>0.05 *vs.* MOD group and [f]p>0.05 *vs.* MOD group**

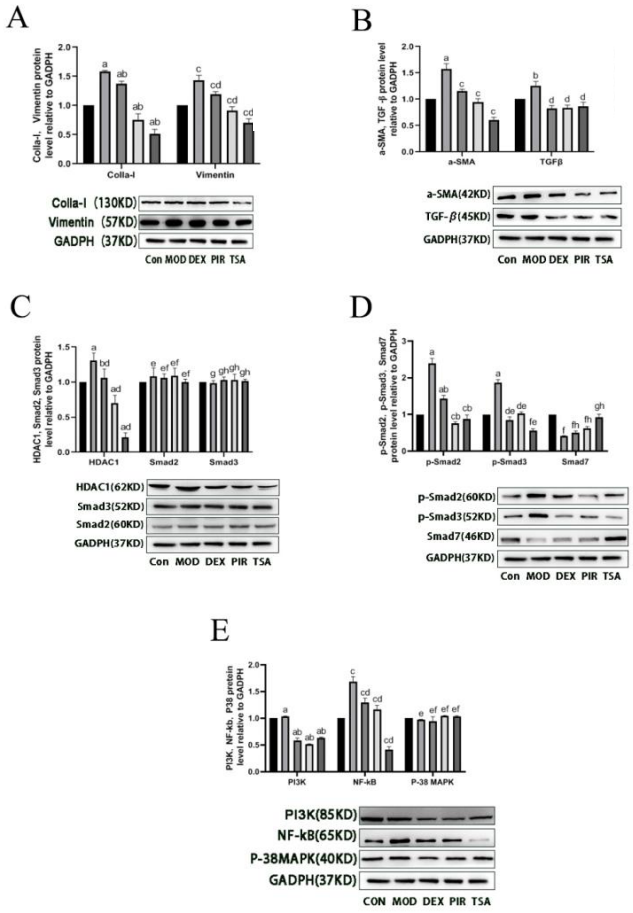


**Fig. 5: Protein expression in the lung tissue of mice in each group**

**Note: (A) Level of collagen-I, vimentin protein; (B) α-SMA, TGF-β protein; (C) HDAC1, Smad2, Smad3 protein; (D) p-Smad2, p-Smad3, Smad7 protein and (E) PI3K, NF-κB, p-38MAPK protein analyzed by Western blot in each group of mice. Values are expressed as mean±SD, [a]p<0.05 *vs.* CON; [b]p<0.05 *vs.* MOD group; [c]p<0.05 *vs.* CON; [d]p<0.05 *vs.* MOD group; [e]p<0.05 *vs.* CON; [f]p<0.05 *vs.* MOD group; [g]p<0.05 *vs.* CON; [h]p<0.05 *vs.* MOD group, ( ) CON; ( ) MOD; ( ) DEX; ( ) PIR and ( ) TSA groups**

Real Time-Polymerase Chain Reaction (RT-PCR) was used to detect the changes of collagen-I mRNA, vimentin mRNA and α-SMA mRNA in the lung tissue of mice in each group on the 7th, 14th and 28th d after modeling. The expression of α-SMA mRNA in the MOD group increased gradually with time. The expression of α-SMA mRNA in the three drug intervention groups peaked on the 14th d after modeling (fig. 6A).

The expression of collagen-I mRNA in the MOD group increased gradually with time and the expression level of collagen-I mRNA in the three drug intervention groups decreased in varying degrees after 7 d (fig. 6B).

Vimentin mRNA in the MOD group changed with time and peaked on the 14th d. The expression of vimentin mRNA in the three drug intervention treatment groups was the most in DEX group (fig. 6C).

Results of WGCNA and KEGG pathway enrichment analysis was shown here. The R/Bioconductor software package was used to extract the data of three GEO Series (GSE) files in Gene Expression Omnibus (GEO) database. The GEO object returned by GEO function is composed of gene expression matrix, clinical characteristics and probe set, and then the data are analyzed. It can be seen that the three colors in the figure represent three data files respectively (fig. 7A). The R language in Surrogate Variable Analysis (SVA) package is used to remove the batch effect. Before cross platform standardization, the expression values of the two data sets are log2 transformed. We chose combat to remove the batch effect in three databases. The combat method is used to normalize the differences between data from different batches or different platforms and principal component analysis is used to evaluate whether the batch effect is removed. It can be seen from the figure that the data in the three color files are mixed together indicating that the batch effect of different data sources is well removed (fig. 7B).

Consistency cluster analysis is used to divide IPF patients into different subgroups. The cluster analysis is carried out by Spearman k-means algorithm, the maximum cluster number is set to 10 and the final cluster number is determined by the consistency matrix and cluster consistency score (>0.8). It can be seen from the figure that when they are grouped into two categories, the consistency score is greater than 0.8 and the stability is better. Therefore, the population in the above data is divided into two subgroups (fig. 7C).

Wilcoxon rank-sum test compared the differences in age and gender between the two subgroups. The results showed that there was no significant difference in age and gender between the two subgroups (fig. 7D).

Through the comparative analysis between the CON group and the two subgroups, the specific up-regulated genes were determined and the differential expression was tested by Wilcoxon rank-sum test. After Benjamini-Hochberg adjustment, p value<0.05 and mean absolute difference>0.2. For a specific gene, the difference in the mean is calculated by subtracting the mean of the normal CON group from each subgroup. The results show that they all have converge to the left and the degree of density and sparsity represent the degree of difference (fig. 7E).

WGCNA determines the biological function of each module by identifying modules with potential functions in subgroups. The soft threshold of scale-free network is determined according to the maximum $R^2$ value. The similarity of topological overlap matrix was used to evaluate the distance between gene pairs. The average method and dynamic method were used for hierarchical cluster analysis, the cluster tree was established, the genes were divided into modules and finally four functional modules were determined. The Spearman method in WGCNA software package was used to calculate the correlation coefficient and corresponding p value between clinical features and functional modules.

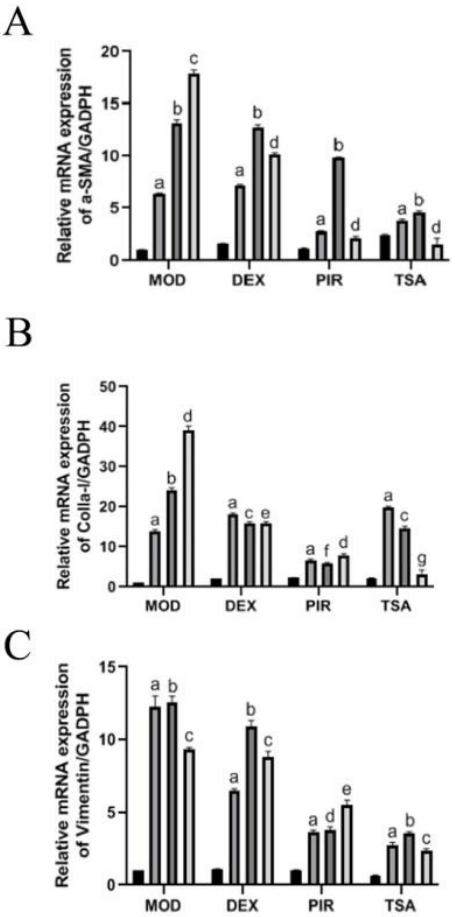


**Fig. 6: (A) Expression of α-SMA mRNA; (B) Collagen-I mRNA and (C) Vimentin mRNA determined by RT-PCR in lung tissue of mice in each group at 0, 7, 14 and 28 d after modeling**

**Note: ap<0.05 *vs.* 0 d group; [b]p<0.05 *vs.* 7 d group; [c]p<0.05 *vs.* 14 d MOD group, [d]p<0.05 *vs.* 14 d group; [e]p<0.05 *vs.* 28 d group; [f]p<0.05 *vs.* 14 d PIR group; [g]p<0.05 *vs.* 28 d TSA group; ( ▬ ) 0 d; ( ▭ ) 7 d; ( ▬ ) 14 d and ( ▭ ) 28 d**

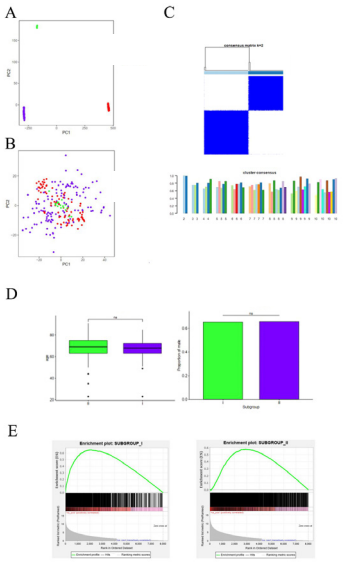


**Fig. 7: The results of differentially expressed gene analysis**
**Note: (A, B) The R/Bioconductor software package was conducted to extract the data of three GSE files in GEO database, ( ) GSE135099; ( ) GSE33566 and ( ) GSE49072; (C) The consistency cluster analysis was used to divide IPF patients into different subgroups, ( ) 1; ( ) 2; (D) The Wilcoxon rank-sum test was applied to compare the differences in age and gender between the two subgroups, ( ) I; ( ) II and (E) The enrichment plots for different groups**

There are 1503 genes in brown, 740 genes in grey, 208 genes in red and 1030 genes in turquoise. Red indicates that the genes in the module are highly expressed in this group and blue indicates that the genes in the module are low expressed in this group. It shows that the genes in brown are low expressed in group I and high expressed in group II. There was no significant difference in the expression of genes in grey section. The genes in the red section are low expressed in group I and high expressed in group II. The gene in turquoise is highly expressed in group I and low expressed in group II (fig. 8A).

Over Characterization Enrichment Analysis (OEA) is based on hypergeometric test (or Fisher test). 10 most important KEGG pathways are selected for each section and the genome from KEGG pathway is downloaded from Molecular Signatures Database (MSigDB). In the fig. 8B, (▲) represents $p<0.05$ and (●) represents $p>0.05$. The more red the color, the smaller the p value and the more significant the difference, the bluer the color, the greater the p value and the difference is less significant. It can be seen from the figure that pathways such as ribosome, amyotrophic lateral sclerosis, RNA transport, spliceosome, Coronavirus Disease 2019 (COVID-19), Parkinson's disease, prion disease, Huntington disease, Epstein-Barr virus infection are obviously enriched in the brown gene module; Epstein-Barr virus infection, phagosome, antigen processing and presentation, viral myocarditis, cell adhesion molecules and other pathways were significantly enriched in the green gene module; ribosome, amyotrophic lateral sclerosis, RNA transport, COVID-19, Parkinson's disease, prion disease, Huntington disease and other pathways were significantly enriched in the red gene module; pathways such as PI3K/Protein Kinase B (Akt) signaling pathway, estrogen signaling pathway, Extracellular Matrix Protein (ECM) receiver interaction, calcium signaling pathway, neuroactive live receiver interactions are significantly enriched in the turquoise gene module (fig. 8B).

Bleomycin (BLM) is a broad-spectrum antitumor drug, which is widely used in the study of pulmonary fibrosis model[14-17]. Many studies have shown that the lung tissue of C57BL/6 mice is highly sensitive to bleomycin, which makes the performance of pulmonary fibrosis obvious. Therefore, it is used for the study of pulmonary fibrosis in mice[18-20]. The traditional modeling method is direct intratracheal injection or tail vein injection of bleomycin. The former is to cut the neck skin and subcutaneous tissue and inject bleomycin into the trachea after exposing the trachea. It has the disadvantages of easy infection, high mortality and long anesthesia time in mice; caudal vein injection is difficult and easy to cause caudal ulceration[21-23]. The above methods mostly affect the level of cytokines *in vivo* due to exogenous factors such as infection or stress. Therefore, we use one-time intranasal injection of bleomycin, which has relatively small exogenous injury, simple and convenient operation and small dose.

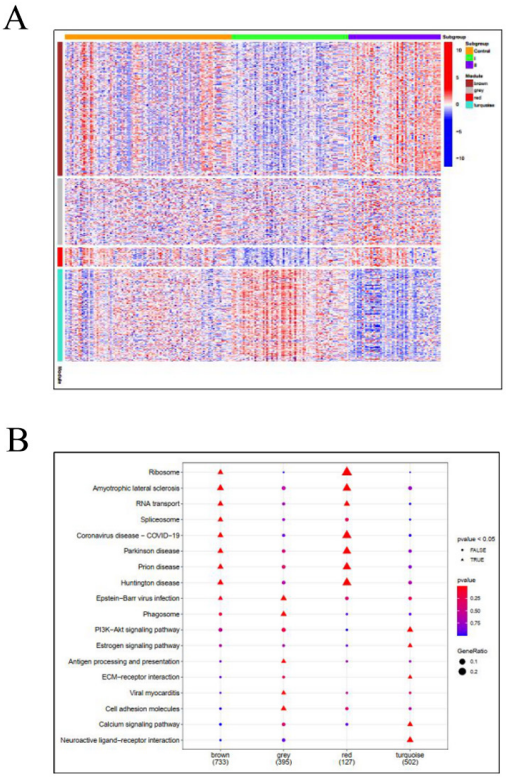


**Fig. 8: The results of WGCNA and KEGG pathway enrichment analysis**
**Note: (A) WGCNA was established to determine the biological function of each module by identifying modules with potential functions in subgroups and (B) The 10 most important KEGG pathways were selected for each section**

In this part of the experiment, it was found that one-time intranasal injection of bleomycin (5 mg/kg) can successfully simulate the model of pulmonary fibrosis. After modeling, the activity and diet of mice were basically normal. From the 5$^{th}$ d, the reaction was slow, the eating was reduced, the spirit was depressed and the activity was reduced; with the passage of time, the above manifestations were further aggravated, accompanied by shortness of breath and the weight was significantly reduced compared with that before modeling. The results of HE staining showed that the lung tissue of mice showed fibrosis, a large number of inflammatory cells dominated by lymphocytes infiltrated in the early stage and thrombosis was observed in the vascular cavity. With the extension of time, on the 14$^{th}$ d of modeling, the alveolar septum widened, bleeding was seen in the alveolar cavity, thrombus was still seen in the small vascular cavity, but it decreased in the early stage. The inflammatory cell infiltration was mainly lymphocytes and macrophages, and the type II alveolar epithelial cells proliferated. On the 28$^{th}$ d of modeling, the lung tissue structure was further damaged, the alveolar cavity fused, a large number of collagen fibers were deposited in the lung stroma and the alveolar cavity could not be identified. A large number of basal cells showed mass proliferation, alveolar cavity bleeding, type II alveolar epithelial cell proliferation was more obvious and a large number of macrophage cells infiltrated in the lung tissue. Masson's staining showed that a large number of blue collagen fibers were deposited in the lung stroma, alveolar septum, airway and blood vessels of the MOD group. The deposition of collagen fibers in the DEX group was significantly higher than that in the CON group, PIR group and TSA group. In each group, TSA group had the least lung injury and the least collagen fiber deposition. The results of hydroxyproline content showed that the content of hydroxyproline in lung tissue of mice in each group was significantly higher than that in the CON group and increased with time. There was no significant difference in the content of hydroxyproline between DEX group and MOD group. The content of hydroxyproline in PIR group and TSA group decreased significantly compared with MOD group, especially in TSA group.

The results showed that the expression of vimentin, collagen-I and α-SMA in the MOD group was significantly higher than that in the CON group and the expression gradually increased with time. The expression of these proteins in DEX group, PIR group and TSA group was lower than that in MOD

group, and the expression in TSA group was the least.

TGF-β1 has a strong role in causing pulmonary fibrosis. It has always been a research hotspot in the field of pulmonary fibrosis and plays an important role in the occurrence and development of pulmonary fibrosis. A large number of studies have confirmed that in the mouse pulmonary fibrosis model induced by bleomycin, TGF-β1 mRNA expression is significantly increased and can play an independent role in the progression of pulmonary fibrosis[24]. TGF-β1/Smads pathway is the most important intracellular signal transduction pathway known at present. The activation of this pathway is closely related to Epithelial-Mesenchymal Transition (EMT)[25]. Its transmission process is exogenous stimulation acts on the body to promote the secretion of inflammatory cells to produce TGF-β1, with TGF on cell membrane-β Type II receptor which binds to make type I receptor phosphorylated and the activated type I receptor phosphorylates its downstream Smad2 and Smad3 proteins. After phosphorylation, Smad2 and Smad3 are separated from the receptor complex, react with Smad4 protein and then transform into heteropolymer complex, immerse into the nucleus and act on the activation of collagen and CREB-Binding Protein (CBP)/p300 transcription coactivators, further affect the target gene transcription[26], make a large amount of ECM deposit, increase protein expression and then destroy the alveolar structure and promote pulmonary fibrosis[27,28]; Smad7 is TGF-β1, the negative regulator of Smads signaling pathway can inhibit the phosphorylation of Smad2 and Smad3, and then indirectly inhibit pulmonary fibrosis. In this experiment, the results of Western blot also showed that TGF-β1, p-Smad2 and p-Smad3 in the MOD group were significantly higher than those in the CON group, the level of Smad7 protein was significantly lower than that in the CON group and there was no significant difference in the levels of Smad2 and Smad3 protein. In the three drug intervention groups, TGF-β1, p-Smad2, p-Smad3 and other proteins decreased in varying degrees and the expression of Smad7 protein increased in varying degrees, especially in TSA group. Therefore, the activation of TGF-β1/Smads pathway plays a key role in bleomycin induced pulmonary fibrosis in C57BL/6 mice and TSA can improve pulmonary fibers by inhibiting the activation of this pathway.

HDACi is a new type of antitumor drug based on epigenetic theory. It has good antitumor effect and good prospect of application because of its broad spectrum, high efficiency and low toxicity. At present, the new drugs on the market and under development, such as vorinostat (Suberoylanilide Hydroxamic Acid (SAHA)), belinostat, TSA and romidicin, are used to treat skin T-cell lymphoma[29]. TSA is the first natural hydroxamic acid found to inhibit the activity of HDACs. It belongs to non-selective HDACi, which can inhibit the activity of class I and class II HDACs[30]. DEX, PIR and TSA were used as intervention measures to compare the intervention effects of three drugs. The results showed that the above drugs had an effect on the expression of HDAC1. In TSA group, the expression levels of HDAC1, p-Smad2 and p-Smad3 protein decreased significantly and the level of Smad7 protein increased significantly, indicating that the change of HDAC1 activity was involved in the process of pulmonary fibrosis. TSA can inhibit the activity of HDAC1 and then TGF-β1/Smads pathway to inhibit pulmonary fibrosis. The pathological results of mouse lung tissue also confirmed the findings of appeal. In TSA group, the lung tissue injury was the least, the interstitial protein deposition was the least, but there was a large number of macrophage infiltration. It can be seen that the inhibitory effect of TSA on pulmonary fibrosis is related to the over activation of macrophages or there is a correlation between the change of HDAC1 activity and macrophage activation, which still needs to be further studied.

Through the above research results, we need to have a deep understanding of HDAC. HDAC1 only exists in the nucleus of the body, which is class I HDAC and its function is to deacetylate Smad7[31]; In addition, class I HDAC also includes HDAC2, HDAC3, HDAC8, class II HDAC includes HDAC4, HDAC5, HDAC6, HDAC7, HDAC9 and HDAC10, while Sirtuin (SIRT) 1-7 and HDAC11 belong to class III and IV respectively. They have different protein affinity, so that they have different effects; HDACi could not inhibit SIRT1-7. Histone Acetyltransferases (HATs) can specifically transfer the acetyl group of acetyl coenzyme A, acetylate the target lysine residue at the N-end of polypeptide chain, neutralize the positive charge of protein, dissociate Deoxyribonucleic Acid (DNA) octamer and activate gene transcription[11]; In addition, non-histone acetylation can also be catalyzed by HATs[32]. Deacetylation and acetylation show a dynamic balance of positive and negative reactions in the physiological state of the body. Under pathological conditions, this dynamic balance will be

broken and tend to acetylation or deacetylation, so as to change the physiological function or stability of proteins, leading to the occurrence and progress of diseases such as tumor or fibrosis[33]. The results showed that the expression of HDAC1 in the MOD group was significantly higher than that in the CON group; Korfei *et al.*[34] also found that HDAC1 protein expression increased and activity increased in the lung tissue experiment of IPF patients, suggesting that there is an imbalance between acetylation and deacetylation caused by increased HDAC1 activity in fibrotic diseases. In this experiment, the Western blot results also showed that the expression of HDAC1 protein in the MOD group was significantly higher than that in the CON group. Among the three drug intervention groups, the expression of HDAC1 protein decreased in varying degrees than that in the MOD group, especially in TSA group, which further showed that TSA could reduce the expression of HDAC1 protein and inhibit TGF by inhibiting the activity of HDAC1-β1/Smads pathway, reduce the expression of p-Smad2 and p-Smad3 protein and promote the expression of Smad7 protein to inhibit fibrosis.

This study also observed that the expression of PI3K, NF-κB and other proteins increased significantly in the MOD group, but decreased in DEX group, PIR group and TSA group, while there was no significant difference in the expression of p38-MAPK protein in each stage, indicating that PI3K and NF-κB pathways are involved in the process of pulmonary fibrosis. As a nuclear transcription factor, NF-κB mainly exists in the cytoplasm. Under the action of stimulating factors, NF-κB can be activated into the nucleus, promote the transcription of cell adhesion molecules, cytokines, growth factors, anti-apoptosis and other genes, and play an important role in inflammatory response and immune regulation[35]. PI3K/Akt signaling pathway plays a key regulatory role in cell proliferation, differentiation, apoptosis and autophagy[36] and is an important signaling pathway for tumor diseases. This part of the experiment shows that the pathogenesis of pulmonary fibrosis is similar to tumor diseases or the activation of some pathways can lead to both tumor and pulmonary fiber. It also shows that TSA not only has anti-lymphoma effect, but also has anti-fibrosis molecular mechanism.

Among the three drugs compared in this study, DEX, as a long-acting corticosteroid hormone, has the effects of anti-inflammatory, anti-toxic, anti-allergic and anti-rheumatism and is used in the treatment of many diseases. However, it has little effect in the treatment of pulmonary fibrosis. The study also observed that the lung tissue of DEX group was the most severely injured. The expression of interstitial proteins and corresponding mRNA such as vimentin, collagen-I and α-SMA decreased significantly compared with the MOD group but increased significantly compared with the PIR group and TSA group, indicating that the effect of DEX in the treatment of pulmonary fibrosis was poor. There are many experimental studies on PIR *in vitro*. It can inhibit the overexpression of fibrogenic factors such as basic Fibroblast Growth Factor (bFGF) and Platelet-Derived Growth Factor (PDGF), and recently play the role of anti-oxidation, anti-inflammatory and anti-fibrosis, effectively inhibit collagen synthesis, fibroblast proliferation and reduce matrix extracellular deposition[37-39]. Although it can alleviate pulmonary fibrosis to a certain extent, it cannot inhibit the progression of pulmonary fiber. As an inhibitor of HDAC, TSA significantly inhibited bleomycin induced pulmonary fibrosis in this part of the experiment.

Gene expression regulation can be achieved through epigenetic modification. Based on specific gene nucleotide sequence, covalent modification, including DNA ubiquitination, phosphorylation, methylation and acetylation, can change gene expression and finally change cell function[40]. This study also shows that the balance between histone acetylation and deacetylation plays an important role in the occurrence and development of IPF. HDACi will bring new hope for the treatment of IPF.

During the occurrence and development of pulmonary fibrosis, there was imbalance of coagulation system and varying degrees of pulmonary hemorrhage. The activation of macrophages is involved in the occurrence and development of pulmonary fibrosis. TSA can inhibit TGF by inhibiting the activity of HDAC1-β1/Smads pathway which significantly inhibited the progression of pulmonary fibrosis where DEX cannot delay or improve pulmonary fibrosis.

**Author's contributions:**

Qian Zhang, Ze-Xin Guo and Jing Zhang contributed equally to this work. Ze-Xin Guo and Jing Zhang collected the animal materials and performed the experiments; Dong-Liang Yang, Jie Cao and Shuo Li analyzed the results and Qian Zhang supervised the study and Bo Zhang wrote the article.

**Funding:**

This study was supported by Tianjin New Century Talent Project, China.

**Conflict of interests:**

The authors declare that they have no competing interests.

## REFERENCES

1. Gu L, Zhu YJ, Yang X, Guo ZJ, Xu WB, Tian XL. Effect of TGF-β/Smad signaling pathway on lung myofibroblast differentiation 4. Acta Pharmacol Sin 2007;28(3):382-91.
2. Chambers DM, Moretti L, Zhang JJ, Cooper SW, Chambers DM, Santangelo PJ, *et al.* LEM domain-containing protein 3 antagonizes TGFβ-SMAD2/3 signaling in a stiffness-dependent manner in both the nucleus and cytosol. J Biol Chem 2018;293(41):15867-86.
3. Shi Y, Massagué J. Mechanisms of TGF-β signaling from cell membrane to the nucleus. Cell 2003;113(6):685-700.
4. Verrecchia F, Mauviel A. Transforming growth factor-β and fibrosis. World J Gastroenterol 2007;13(22):3056-62.
5. Beyer TA, Narimatsu M, Weiss A, David L, Wrana JL. The TGF-β superfamily in stem cell biology and early mammalian embryonic development. Biochim Biophys Acta Gen Subj 2013;1830(2):2268-79.
6. Itoh S, Itoh F, Goumans MJ, Ten Dijke P. Signaling of transforming growth factor-β family members through Smad proteins. Eur J Biochem 2000;267(24):6954-67.
7. Mann BS, Johnson JR, He K, Sridhara R, Abraham S, Booth BP, *et al.* Vorinostat for treatment of cutaneous manifestations of advanced primary cutaneous T-cell lymphoma. Clin Cancer Res 2007;13(8):2318-22.
8. McDermott J, Jimeno A. Belinostat for the treatment of peripheral T-cell lymphomas. Drugs Today 2014;50(5):337-45.
9. King JR TE, Schwarz MI, Brown K, Tooze JA, Colby TV, Waldron Jr JA, *et al.* Idiopathic pulmonary fibrosis: Relationship between histopathologic features and mortality. Am J Respir Crit Care Med 2001;164(6):1025-32.
10. Deroanne CF, Bonjean K, Servotte S, Devy L, Colige A, Clausse N, *et al.* Histone deacetylases inhibitors as anti-angiogenic agents altering vascular endothelial growth factor signaling. Oncogene 2002;21(3):427-36.
11. Pang M, Zhuang S. Histone deacetylase: A potential therapeutic target for fibrotic disorders. J Pharmacol Exp Ther 2010;335(2):266-72.
12. Minucci S, Pelicci PG. Histone deacetylase inhibitors and the promise of epigenetic (and more) treatments for cancer. Nat Rev Cancer 2006;6(1):38-51.
13. Szapiel SV, Elson NA, Fulmer JD, Hunninghake GW, Crystal RG. Bleomycin-induced interstitial pulmonary disease in the nude, athymic mouse. Am Rev Respir Dis 1979;120(4):893-9.
14. Li YF, Hu CP and Li F. Research progress of animal models of pulmonary fibrosis. Zhongnan J Med Sci 2016;44(2):211-5.
15. Xie XY, Wang JK, Deng PP, Zheng XL, Qian Sy, Li M. Research progress of bleomycin as antitumor antibiotic. Coal Chem Ind 2016;39(3):76-8.
16. Della Latta V, Cecchettini A, Del Ry S, Morales MA. Bleomycin in the setting of lung fibrosis induction: From biological mechanisms to counteractions. Pharmacol Res 2015;97:122-30.
17. Tu CL, Liu X, Zheng XB, Yu JL, Zhu SQ, Su MH, *et al.* Intravenous injection of bleomycin induces pulmonary fibrosis in mice: A stability evaluation. Chin J Tissue Eng Res 2015;19(40):6436-43.
18. Xiao Y, Zhang JW, Wang WM. Discussion on the establishment of animal model of idiopathic pulmonary interstitial fibrosis. Jilin Med J 2016;37(4):941-3.
19. Song SF, Zhang XY. Comparison of C57BL/6 induced by bleomycin and ICR mouse pulmonary interstitial fibrosis model. Chin J Exp Anim 2010;18(4):289-91.
20. Song GQ, Xu ZW, Li Z, Li XS, Zhang XY. Comparative study on pulmonary fibrosis model induced by bleomycin in three strains of mice. China J Mod Med 2017;27(4):13-6.
21. Li W, Hu Y, Yuan W, Li L, Huang W. Comparison of two mouse models of lung fibrosis induced by intratracheal instillation and intratracheal aerosol administration of bleomycin. Nan Fang Yi Ke Da Xue Xue Bao 2012;32(2):221-5.
22. Meng J, Peng ZZ, Tao LJ. Comparative study on mouse pulmonary fibrosis model induced by low-dose multiple tail vein injection and intratracheal instillation of bleomycin. J Cent South Univ 2013;38(12):1228-32.
23. Chen MY, Lin S, Du P, Li CC, Meng A. Establishment of murine pulmonary fibrosis model induced by repetitive intratracheal administration of bleomycin. China Med Her 2017;14(2):8-11.
24. Kan B, Jian X, Zhou Q, Wang J, Yu G, Sun J, *et al.* Effect of transforming growth factor-β1 on acute lung injury caused by paraquat. Mol Med Rep 2014;9(4):1232-6.
25. Han YY, Shen P, Chang WX. Involvement of epithelial-to-mesenchymal transition and associated transforming growth factor-β/Smad signaling in paraquat-induced pulmonary fibrosis. Mol Med Rep 2015;12(6):7979-84.
26. Rahimi RA, Leof EB. TGF-β signaling: A tale of two responses. J Cell Biochem 2007;102(3):593-608.
27. Datto M, Wang XF. Ubiquitin-mediated degradation: A mechanism for fine-tuning TGF-β signaling. Cell 2005;121(1):2-4.
28. Hayashi H, Abdollah S, Qiu Y, Cai J, Xu YY, Grinnell BW, *et al.* The MAD-related protein Smad7 associates with the TGF-β receptor and functions as an antagonist of TGF-β signaling. Cell 1997;89(7):1165-73.
29. Mann BS, Johnson JR, Cohen MH, Justice R, Pazdur R. FDA approval summary: Vorinostat for treatment of advanced primary cutaneous T-cell lymphoma. Oncologist 2007;12(10):1247-52.
30. Dokmanovic M, Clarke C, Marks PA. Histone deacetylase inhibitors: Overview and perspectives. Mol Cancer Res 2007;5(10):981-9.
31. Simonsson M, Heldin CH, Ericsson J, Grönroos E. The balance between acetylation and deacetylation controls Smad7 stability. J Biol Chem 2005;280(23):21797-803.
32. Choudhary C, Kumar C, Gnad F, Nielsen ML, Rehman M, Walther TC, *et al.* Lysine acetylation targets protein complexes and co-regulates major cellular functions. Science 2009;325(5942):834-40.
33. Pang M, Ma L, Liu N, Ponnusamy M, Zhao TC, Yan H, *et al.* Histone deacetylase 1/2 mediates proliferation of renal interstitial fibroblasts and expression of cell cycle proteins. J Cell Biochem 2011;112(8):2138-48.
34. Korfei M, Skwarna S, Henneke I, MacKenzie B, Klymenko O, Saito S, *et al.* Aberrant expression and activity of histone deacetylases in sporadic idiopathic pulmonary fibrosis. Thorax 2015;70(11):1022-32.

35. Yu H. Nuclear transcription factor NF-κB and pulmonary fibrosis. Chin J Pract Intern Med 2006;26(15):1203-4.
36. Sharma VR, Gupta GK, Sharma AK, Batra N, Sharma DK, Joshi A, *et al.* PI3K/Akt/mTOR intracellular pathway and breast cancer: Factors, mechanism and regulation. Curr Pharm Des 2017;23(11):1633-8.
37. Zhao Y, Zhao MS, Qin J. Research progress of pirfenidone in the treatment of idiopathic pulmonary fibrosis. Contemp Med 2013;19(9):12-3.
38. Chen YQ. Meta-analysis of efficacy and safety of pirfenidone in the treatment of pulmonary fibrosis. J Clin Drug Ther 2016;14(04):13-22.
39. Shao MX. Pirfenidone, a new anti-pulmonary fibrosis drug. Mod Drug Clin 2013;28(3):409-14.
40. Hassell KN. Histone deacetylases and their inhibitors in cancer epigenetics. Diseases 2019;7(4):57.



**This article was originally published in a special issue, "Advanced Targeted Therapies in Biomedical and Pharmaceutical Sciences" Indian J Pharm Sci 2023:85(1) Spl Issue "192-204"**